EUROPEAN ORGANIZATION FOR NUCLEAR RESEARCH

CERN-EP/87-74
April 9th, 1987

Proton and Antiproton Production in Deep Inelastic Muon-Nucleon Scattering at 280 GeV

The European Muon Collaboration

Aachen[1], CERN[2], DESY (Hamburg)[3], Freiburg[4], Hamburg (University)[5], Kiel[6], LAL (Orsay)[7], Lancaster[8], LAPP (Annecy)[9], Liverpool[10], Marseille[11], Mons[12], MPI (München)[13], Oxford[14], RAL (Chilton)[15], Sheffield[16], Torino[17], Uppsala[18], Warsaw[19], Wuppertal[20]

M. Arneodo[17], A. Arvidson[18], J.J. Aubert[11], B. Badelek[19a], J. Beaufays[2], C.P. Bee[8b], C. Benchouk[11], G. Berghoff[1], I. Bird[8c], D. Blum[7], E. Böhm[6], X. de Bouard[9], F.W. Brasse[3], H. Braun[20], C. Broll[9+], S. Brown[10d], H. Brück[20e], H. Calen[18], J.S. Chima[15f], J. Ciborowski[19a], R. Clifft[15], G. Coignet[9], F. Combley[16], J. Coughlan[8g], G. D'Agostini[11], S. Dahlgren[18], F. Dengler[13], I. Derado[13], T. Dreyer[4], J. Drees[20], M. Düren[1], V. Eckardt[13], A. Edwards[20h], M. Edwards[15], T. Ernst[4], G. Eszes[9i], J. Favier[9], M.I. Ferrero[17], J. Figiel[5j], W. Flauger[3], J. Foster[16k], E. Gabathuler[10], J. Gajewski[5], R. Gamet[10], J. Gayler[3], N. Geddes[14g], P. Grafström[18], F. Grard[12], J. Haas[4], E. Hagberg[18], F.J. Hasert[11], P. Hayman[10], P. Heusse[7], M. Jaffré[7], A. Jacholkowska[2], F. Janata[5t], G. Jansco[13i], A.S. Johnson[14m], E.M. Kabuss[4], G. Kellner[2], V. Korbel[3], A. Krüger[5], J. Krüger[20e], S. Kullander[18], U. Landgraf[4], D. Lanske[1], J. Loken[14], K. Long[14n], M. Maire[9], P. Malecki[13], A. Manz[13], S. Maselli[13], W. Mohr[4], F. Montanet[11], H.E. Montgomery[2o], E. Nagy[9i], J. Nassalski[19p], P.R. Norton[15], F.G. Oakham[15q], A.M. Osborne[2], C. Pascaud[7], B. Pawlik[13], P. Payre[11], C. Peroni[17], H. Peschel[20], H. Pessard[9], J. Pettingale[10], B. Pietrzyk[11], B. Poensgen[5], M. Pötsch[20], P. Renton[14], P. Ribarics[9i], K. Rith[4c], E. Rondio[19a], A. Sandacz[19p], M. Scheer[1], A. Schlagböhmer[4], H. Schiemann[5], N. Schmitz[13], M. Schneegans[9], M. Scholz[1], M. Schouten[13], T. Schröder[4], K. Schultze[1], T. Sloan[8], H.E. Stier[4], M. Studt[5], G.N. Taylor[14], J.M. Thénard[9], J.C. Thompson[15], A. de la Torre[5r], J. Toth[9i], L. Urban[1], L. Urban[9i], W. Wallucks[4], M. Whalley[16s], S. Wheeler[16], W.S.C. Williams[14], S.J. Wimpenny[10n], R. Windmolders[12], G. Wolf[13].

(Submitted to Zeitschrift für Physik C)

Abstract: New results on proton and antiproton production in the target and current fragmentation regions of high energy muon-nucleon scattering are presented. Proton and antiproton production is investigated as a function of Feynman x and rapidity. No significant difference is observed between production on hydrogen and deuterium targets. Correlations between pp, $p\bar{p}$ and $\bar{p}\bar{p}$ pairs are analysed and the results are compared with the predictions of the Lund fragmentation model.

For footnotes see next page

Addresses

1) III. Physikalisches Institut A, Physikzentrum, RWTH, D-5100 Aachen, Federal Republic of Germany
2) CERN, CH-1211 Geneva 23, Switzerland
3) DESY, D-2000 Hamburg, Federal Republic of Germany
4) Fakultät für Physik, Universität Freiburg, D-7800 Freiburg, Federal Republic of Germany
5) II. Institut für Experimentalphysik, Universität Hamburg, D-2000 Hamburg, Federal Republic of Germany
6) Institut für Kernphysik, Universität Kiel, D-2300 Kiel, Federal Republic of Germany
7) Laboratoire de l'Accélérateur Linéaire, Université de Paris-Sud, F-91405 Orsay, France
8) Department of Physics, University of Lancaster, Lancaster LA1 4YB, UK
9) LAPP, IN2P3, F-74019 Annecy-le-Vieux, France
10) Oliver Lodge Laboratory, Department of Physics, University of Liverpool, Liverpool L693BX, UK
11) Centre de Physique des Particules, Faculté des Sciences de Luminy, F-13288 Marseille, France
12) Faculté des Sciences, Université de l'Etat à Mons, B-7000 Mons, Belgium
13) Max-Planck-Institut für Physik und Astrophysik, D-8000 München, Federal Republic of Germany
14) Nuclear Physics Laboratory, University of Oxford, Oxford OX13RH, UK
15) Rutherford and Appleton Laboratory, Chilton, Didcot OX110QX, UK
16) Department of Physics, University of Sheffield, Sheffield S37RH, UK
17) Istituto di Fisica, Università di Torino, I-10125, Italy
18) Gustav Werners Institut, University of Uppsala, S-75121 Uppsala, Sweden
19) Physics Institute, University of Warsaw, and Institute for Nuclear Studies, PL-00681 Warsaw, Poland
20) Fachbereich Physik, Universität Wuppertal, D-5600 Wuppertal, Federal Republic of Germany

a) University of Warsaw, Poland.
b) Now at University of Liverpool, England.
c) Now at MPI für Kernphysik, Heidelberg, Germany.
d) Now at TESA S.A., Renens, Switzerland.
e) Now at DESY, Hamburg, Germany.
f) Now at British Telecom, London, England.
g) Now at RAL, Chilton, Didcot, England.
h) Now at Jet, Joint Undertaking, Abingdon, England.
i) Permanent address: Central Research Institute for Physics of the Hungarian Academy of Science, Budapest, Hungary.
j) Now at Institute of Nuclear Physics, Krakow, Poland.
k) Now at University of Manchester, England.
l) Now at Krupp Atlas Elektronik GmbH, Bremen, Germany.
m) Now at SLAC, Stanford, California, USA.
n) Now at CERN, Genève, Switzerland.
o) Now at FNAL, Batavia, Illinois, USA.
p) Institute for Nuclear Studies, Warsaw, Poland.
q) Now at NRC, Ottawa, Canada.
r) Now at Universidad Nacional, Mar del Plata, Argentina.
s) Now at University of Durham, England.
t) Now at Beiersdorf AG, Hamburg, Germany.
+) Deceased.

1 Introduction

Deep inelastic lepton-nucleon scattering is usually described in the framework of the Quark Parton Model (QPM), where the exchanged virtual photon interacts with one of the target nucleon constituents resulting in a current jet due to the fragmentation of the struck quark and a target jet containing the target remnants. So far this fragmentation of partons into hadrons has been described only by phenomenological models such as the Field-Feynman model [1], the Lund model [2] or QCD colour singlet cluster fragmentation models [3].

Baryon production in charged lepton-nucleon scattering may stem from two sources. Earlier experiments at relatively low energy found baryons originating directly from the target remnants (for a summary see ref. [4]). At higher energies studies on deep inelastic scattering by the EMC collaboration [5] and on the e^+e^- annihilation reaction at PETRA [6] and PEP [7] have shown that additional baryons and antibaryons are produced in the fragmentation chain. In the present analysis proton and antiproton production is observed both in the fragmentation of the target remnant system and in the fragmentation of the struck quark.

Of specific interest in the study of baryon production is the way in which diquark-antidiquark pairs can be produced in the fragmentation chain. As a first attempt [8] the Lund model assumed that diquark pairs are produced in a similar way to quark pairs, but are suppressed by a factor related to the higher mass of the diquarks. In a more recent version [9] a mechanism proposed by Casher et al. [10] was introduced in order to describe the excess of protons over antiprotons at high $z = E_h/\nu$ and x_{Bj} observed in a previous experiment of the EMC [5].

The experiment, on which we report here, allowed the reconstruction of hadrons in almost the entire solid angle in the centre of mass system of the virtual photon and the target nucleon (CMS) and the identification of protons and antiprotons over large ranges of laboratory momentum. Results on the production of strange neutral baryons [11] and on charged baryons [12], the latter being based on only part of the present statistics, have

already been published.

In this paper results on the production of protons and antiprotons in deep inelastic muon scattering off hydrogen and deuterium targets are presented. In particular, the single particle distributions in terms of the longitudinal hadron variables are presented and a comparison is made of the fragmentation from hydrogen and deuterium targets. This paper also presents the first obervation in high energy deep inelastic scattering of proton-proton, proton-antiproton and antiproton-antiproton pair production.

The results are compared with a recent version of the Lund model (JETSET62) [13]. The two most relevant parameters for baryon production in this model are:

$$p_{qq}/p_q = 0.10 \quad \text{and}$$
$$p_{bmb} = 0.5$$

where p_{qq}/p_q is the relative probability to produce a diquark pair instead of a quark pair and p_{bmb} determines the relative occurence of baryon-antibaryon pairs with a meson in between in the fragmentation chain. All other parameters in the program were set to their default values.

In deep inelastic muon-nucleon scattering the event kinematics are described by the four momenta $k = (E_\mu, \mathbf{p})$ and $k' = (E_{\mu'}, \mathbf{p}')$ of the incoming and scattered muon, $\mathbf{p}$ and $\mathbf{p}'$ forming the muon scattering angle Θ_μ. The four momentum squared of the exchanged virtual photon is $-Q^2 = (k - k')^2$ and the energy transferred in the laboratory system is $\nu = E_\mu - E_{\mu'}$. The Bjorken scaling variable is defined as the ratio $x_{Bj} = Q^2/2M_p\nu$, where M_p is the proton mass. The effective mass W of the hadronic final state is given by $W^2 = M_p^2 - Q^2 + 2M_p\nu$.

The longitudinal distributions of the final state hadrons are described in terms of $x_F = 2p_{||}/W$ (x-Feynman) and $y_{cms} = \frac{1}{2}\ln[(E+p_{||})/(E-p_{||})]$ (rapidity), where $p_{||}$ is the momentum component parallel to the virtual photon and E the energy in the

centre of mass system of the virtual photon and the target nucleon.

2 Experimental Procedure

Since the apparatus [14] and the analysis procedure [12] are described in former publications, we will only discuss here the components essential for the present analysis. The data were taken using the CERN SPS M2 μ^+ beam at an incident muon energy of 280 GeV. The muons were scattered off a 1 m long target filled with either liquid hydrogen or deuterium. The target was surrounded by a streamer chamber located in a superconducting magnet. Outside the streamer chamber tracks were measured in proportional chambers and drift tubes. Tracks with higher momenta were detected in the forward spectrometer, consisting of a conventional magnet and further proportional and drift chambers.

Proton identification was performed with a system consisting of a time of flight hodoscope counter system (TOF), two Aerogel Cerenkov counters (CA) and two gas Cerenkov counters (C0 - filled with neopentane or freon, C1 - filled with nitrogen), all placed in the vertex spectrometer. A large gas Cerenkov counter (C2) filled with neon identified fast protons of momenta up to 80 GeV in the forward spectrometer. In fig. 1a the momentum ranges, where protons can be separated unambiguously from charged pions and kaons are shown, together with the acceptances of the counters. Nearly the entire momentum range from 600 MeV up to 80 Gev is covered, except for a hole between 4 and 10 GeV. When the laboratory momentum distribution is transformed into a CMS variable such as x_F the clear limits between the counters are smeared out. A region of low acceptance remains, however, in the centre as shown in fig. 1b. In general the different counters contribute to the proton identification over the following intervals in x_F: TOF: -0.9 to -0.2, CA: -0.3 to 0, C0: -0.1 to 0.3, C1: 0 to 0.7 and C2: 0.3 to 0.7.

Since tracks with momenta below 600 MeV in the laboratory system could not reach the TOF counters, we applied a general momentum cut of 600 MeV to the data and did not correct for losses

due to this cut. The same cut was applied to the Lund model in order to obtain predictions comparable with the data.

For each TOF and Cerenkov counter traversed by a track, the probabilities for the four mass hypotheses e, π, K and p are calculated according to the expected and the actually measured signal. For tracks passing more than one counter the probabilities for each mass hypothesis are multiplied. The selection of protons and antiprotons is defined by cuts on these probabilities. The cuts were determined by a Monte Carlo simulation of the counters and adjusted in such a way that a reasonable number of protons and antiprotons is achieved whilst the background of misidentified pions and kaons is kept as small as possible [12]. Table 1 shows the numbers of protons and antiprotons obtained from both targets.

A detailed Monte Carlo simulation of the experiment was used to correct the data in particular for radiative effects, trigger acceptance, acceptance losses and reconstruction efficiencies. Monte Carlo events were generated according to the Lund model, followed by a full simulation of detector responses, and then processed in the same way as real events. We checked that smearing effects in the measured variables due to the inaccuracy of the apparatus are negligible. A global acceptance A(x) for a distribution of protons or antiprotons in a given variable x was calculated as the ratio of the distribution, where the background was not included, obtained after the apparatus simulation to the distribution obtained from the generated events. The acceptance, shown in fig. 1 vs. laboratory momentum and x_F, is dominated by the limited momentum ranges for identification and the geometrical acceptance of the TOF and Cerenkov counters.

The Monte Carlo program was also used to simulate the background in the proton and antiproton signal and to estimate the background distributions, $f_b(x)$. Fig. 2 shows the ratios of the background to the total proton and antiproton signals versus the laboratory momentum and x_F as found in the Monte Carlo simulation. The background consists mainly of misidentified kaons and pions originating from the main vertex and a small amount ($< 5\%$) of hadrons originating from secondary interactions. The former is

given by the product of the probability of misidentification times the frequency of kaons and pions. The mass separation accuracy is given for the TOF counters by the time resolution and in the Cerenkov counters by their efficiency. The contribution from the regions where the fraction of background is large to the total proton and antiproton signal is, however, rather small. The overall background to signal ratio in the data is estimated to be 0.23 (0.28) for protons and 0.26 (0.29) for antiprotons from the H_2 (D_2) target (table 1).

Finally, a measured distribution is corrected according to the formula

$$f_c(x) = (f_m(x) - f_b(x)) \; / \; A(x)$$

where f_c denotes the corrected data and f_m the measured data.

The systematic errors on the normalisation stem mainly from uncertainties in the acceptances of the different counters and in the background rate. They were estimated from comparisons of the data with the Monte Carlo apparatus simulation and found to be approximately $0.2(1-A)A$ for the acceptance and $0.3f_b$ for the background. Thus the systematic error on the yield varies from about 15% for protons identified in the TOF counters to about 25% for protons identified in CA. The systematic error for the average multiplicities is estimated to be 18%.

In order to restrict our data to kinematical regions where radiative corrections and acceptance losses are small, the following cuts in the event variables were used:

Q^2	$>$	4 GeV^2		
20 GeV	$<$	ν	$<$	260 GeV
16 GeV^2	$<$	W^2	$<$	400 GeV^2
ν/E_μ	$<$	0.9		
$E_{\mu'}$	$>$	20 GeV		
θ_μ	$>$	0.5°		
x_{Bj}	$>$	0.02		

The numbers of events surviving these cuts are 25047 for the

hydrogen and 20788 for the deuterium target. For the analysis of proton correlations an upper limit in W^2 of 460 GeV^2 was used to increase the statistics, leaving 26413 and 22043 events on hydrogen and deuterium respectively.

3 Single Particle Distributions

The normalised x_F distributions for protons and antiprotons from hydrogen and deuterium targets are shown, together with the Lund model predictions, in fig. 3. In this figure, as in all the subsequent figures and tables only the statistical errors are shown. The proton distributions exhibit the expected dominance in the backward hemisphere ($x_F < 0$), interpreted as the fragmentation of the target remnants, but show also significant contribution in the forward region ($x_F > 0$). The antiproton distributions are rather symmetric and fall below the proton distributions in the forward hemisphere.

Within the systematic errors quoted above, the data are, in general, reasonably well described by the Lund model. However, the model predicts a higher yield of protons from hydrogen than from deuterium, especially in the backward hemisphere, whereas no significant difference in the yield of protons between the two targets is observed in the data.

Fig. 4 shows the rapidity distribution of the total proton number $N_p - N_{\bar{p}}$, separately for four bins of x_{Bj}. In order to gain statistics, particularly in the current fragmentation region, the data from both targets were combined. The predictions of the Lund model are shown separately for each target, but agree well for $y > 0$. The integral over the distributions in fig. 4, i.e. $\langle N_p - N_{\bar{p}} \rangle$, is 0.395 ± 0.014 (stat.) ± 0.071 (syst.) and does not show any significant x_{Bj} dependence.

A large peak at negative values of rapidity is observed in all intervals of x_{Bj}, corresponding to baryon production from the remnants of the target nucleon. The size of the peak is practically independent of x_{Bj}, while its centre is shifted towards higher values of y when x_{Bj} increases. Since higher values of x_{Bj}

correspond in general to lower values of W^2, as indicated in fig. 4, this effect can be understood as a consequence of the reduced rapidity range. In addition, a small surplus of protons over antiprotons is observed also around y = 1 in the higher x_{Bj} bins ($x_{Bj} > 0.035$). Since in this region of x_{Bj} the scattering is predominantly off a valence quark, the baryon is more likely to contain the struck quark than the antibaryon and the total baryon number is compensated by an antibaryon produced at a lower value of rapidity. This effect vanishes for low x_{Bj}, where scattering is predominantly off a sea quark.

The Lund model describes qualitatively the data in the current fragmentation region, but predicts that the centre of the surplus of protons is at a somewhat higher value of y than in the data. The discrepancy discussed above in the proton yield (especially for the hydrogen target) in the target fragmentation region turns out to stem mainly from the two lower x_{Bj} bins. In addition, in the model, the centre of the peak is shifted in all x_{Bj} bins by roughly one third of a unit in rapidity to lower values compared to the data.

An excess of protons over antiprotons in the forward hemisphere is also predicted by models, where, in a significant number of events, the scattering is off a diquark rather than off a quark (see e.g. ref. [15]). In this case one expects to find, on average, less backward protons in events, where already a proton in the forward hemisphere is observed, than in normal events. In order to check this prediction, the ratio

$$F = \langle n_{p(y<-1)} \rangle_A \; / \; \langle n_{p(y<-1)} \rangle_B$$

of the average multiplicities of protons with a rapidity $y_{cms} < -1$ for two classes of events was computed. Class A consists of the events where a proton with a rapidity $y_{cms} > 0.5$ was identified, and class B consists of all accepted events (including those of class A). The central y_{cms} region is excluded here to obtain a clear separation between the forward and backward hemisphere. The ratio F is practically insensitive to the apparatus acceptance. In the data, F is found to be 0.82 ± 0.11 (0.88 ± 0.16) for the H_2 (D_2) target. The small deviation from unity can be understood by a

reduction of additional baryon-antibaryon pair production in the fragmentation process, also in the backward hemisphere, when a large fraction of the momentum is already taken away by a fast proton. This effect is, with F = 0.95 ± 0.02 (0.87 ± 0.05), well reproduced by the Lund model, which does not contain any special diquark scattering mechanism. Thus the simplest version of such a diquark model is not supported by the data.

4 Average Multiplicities

The increase of the average multiplicities of charged hadrons with W is a well known phenomenon and has also been observed in this experiment [16]. Fig. 5 shows, separately for each target, the average multiplicities of backward ($x_F < 0$) and forward ($x_F > 0$) going protons and antiprotons as a function of W. These multiplicities were determined by integrating the x_F distributions over the intervals accessible to the measurement as shown in fig. 3.

The multiplicities follow the same W dependence for both targets. A rise with W can be seen for antiprotons in both hemispheres and for forward going protons, whilst no clear W dependence for protons in the backward hemisphere is observed. The Lund model (histogram in fig. 5) reproduces well the W dependence of the data, except that it predicts a small rise for backward going protons. As already seen in fig. 3 and 4, the Lund model predicts a higher yield of backward going protons from hydrogen than from deuterium, an effect which is less pronounced in the data.

Fig. 6 shows the ratio of average multiplicities of protons and antiprotons from the deuterium to the hydrogen target as a function of x_{Bj}. The ratio of the total cross sections for scattering on neutrons to scattering on protons is strongly x_{Bj} dependent [17], giving rise to the presumption that a difference in the fragmentation might also show up as a function of x_{Bj}. The data points in fig. 6 are consistent with one for protons in the forward hemisphere. For backward going protons they are below one for small x_{Bj} and rise up to one. For antiprotons the data points

are above one for small x_{Bj} and drop down to one at $x_{Bj} \approx 0.2$, while the Lund model predicts a value of one for all values of x_{Bj}.

5 Correlations

In this section we discuss first the global correlations in the production of pp, $p\bar{p}$ and $\bar{p}\bar{p}$ pairs and secondly investigate some differential distributions of those pairs.

In contrast to the single particle acceptances, which are functions of the apparatus only, the acceptance for particle pairs depends also on their correlations and cannot be evaluated without further assumptions. To reduce this model influence the analysis was restricted to those regions in laboratory momenta, where the acceptance is reasonably good. Therefore all results presented in this section were corrected only for acceptance losses inside this momentum ranges (see fig. 1). For the comparisons with the Lund model, identical cuts were then applied to the Monte Carlo.

The total number of identified pp, $p\bar{p}$ and $\bar{p}\bar{p}$ combinations, as found in the raw data, is given in table 2, together with the corresponding number of background combinations as estimated from the Monte Carlo simulation. As background we count those pairs, where at least one of the particles is misidentified.

Table 3 contains the average pair multiplicities per event together with the Lund model predictions. Since, in the data, there is no significant difference in the results from the two targets, except in the multiplicity of pp combinations, we also give the combined values. We observe slightly more $p\bar{p}$ than pp pairs in the data and a number of $\bar{p}\bar{p}$ combinations more than an order of magnitude smaller. Inside the kinematic restrictions mentioned above, the Lund model predicts a higher yield of $p\bar{p}$ pairs than is found in the data, but a lower multiplicity of $\bar{p}\bar{p}$ pairs.

The correlation in the production of two particles (i, j) is measured with the quantity R, which is defined as

$$R = \frac{\langle n_{ij} \rangle}{\langle n_i \rangle \langle n_j \rangle}$$

for different particle types and as

$$R = \frac{\langle n(n-1) \rangle}{\langle n \rangle^2}$$

if the particles i and j are of the same type. R is expected to be one for uncorrelated production, to approach zero for anticorrelated production and to be larger than one for the case of correlated production, depending on the strength of the correlation.

As can be seen from table 3, R is about 0.2 for pp pairs, showing that additional protons are produced in the fragmentation chain besides the protons from the target remnants. R for $p\bar{p}$ pairs is found to be slightly above one. One expects the production of $p\bar{p}$ pairs to be correlated due to baryon number conservation, as predicted by the Lund model and observed in e^+e^- annihilation [18]. However, in muon-nucleon scattering the measured correlation is strongly reduced due to the large number of combinations of antiprotons with protons from the target remnants. For $\bar{p}\bar{p}$ pairs a value of R compatible with one is found, whereas the Lund model predicts an anticorrelation (R = 0.35). In the interpretation of the differences between the data and the Lund model in the case of $p\bar{p}$ and $\bar{p}\bar{p}$ pairs, the kinematic restrictions of the particle identification has to be borne in mind.

The differential distributions of pair production, e.g. in rapidity, may provide more detailed information on how the

diquarks are formed in the fragmentation chain. For this analysis again the data from both targets were combined in order to gain statistics, but - for clarity - are compared only with the Lund model predictions for a hydrogen target.

A sample of events was selected by requiring an antiproton in the hadronic final state. In order to investigate any differences in the proton distributions in these and average events, the ratio of the rapidity distributions of protons for events with an antiproton to the average of all events was constructed and is shown in fig. 7. The acceptance correction for this ratio is rather small. The correlation of the number of protons in the forward hemisphere with the antiproton trigger is striking. On the other hand, the majority of protons with $y < 0$ stem from the target remants rather than from additional baryon production in the fragmentation process, and thus no correlation is observed in this region. The Lund model prediction, shown by the histogram in fig. 7, describes this correlation well in both hemispheres.

In fig. 8 the distribution of the rapidity distance between two protons or a proton and an antiproton is plotted. The rapidity gap distribution is consistent with being flat for combinations of two protons (Fig. 8a) as well as for pairs of a proton and an antiproton (Fig. 8b), when the proton most likely originates from the target remnant ($y_p < -1$). This suggest that these particles are produced independently in the fragmentation chain. On the other hand, the rapidity gap distribution peaks at zero for $p\bar{p}$ pairs with a forward proton ($y_p > 0.5$) (Fig. 8c), indicating that these particles are produced closely together in the fragmentation chain. The average separation in rapidity is smaller than one unit for these pairs while it is about two units for pp pairs or for $p\bar{p}$ pairs with $y_p < -1$. The shapes of the rapidity gap distributions and the mean rapidity gaps of the $p\bar{p}$ pairs are well reproduced by the Lund model, indicating that the mechanism used to describe the diquark generation is basically compatible with the data.

6 Conclusions

Proton as well as antiproton production from both a hydrogen and a deuterium target are found to show the same behaviour in the x_F distributions. This target independence is also true for the W dependence of the average multiplicities. The multiplicities of antiprotons and forward produced protons exhibit the same significant rise with W. The Lund model is generally in agreement with the data. However it predicts a somewhat higher yield of protons from the hydrogen than from the deuterium target, an effect which is less pronounced in the data.

The size of the observed anticorrelation in the production of pp pairs shows that the dominant source of protons are target remnants but additional protons are produced in the fragmentation chain. Less $p\bar{p}$ pairs are found in the data than predicted by the Lund model. On the other hand, $\bar{p}\bar{p}$ pair production is somewhat underestimated in the Lund model.

The production of protons, in particular in the forward hemisphere, is strongly correlated with antiproton production. For $y_p > 0.5$ $p\bar{p}$ pairs show a strong correlation in rapidity, which is not observed for pp pairs or $p\bar{p}$ pairs with $y_p < -1$. The mechanism of diquark production in the Lund model is compatible with the experimental results.

Acknowledgements

We thank all the people in the various laboratories who have contributed to the construction, operating and analysis of this experiment. In particular we gratefully acknowledge the support of the CERN staff in operating the SPS, M2 muon beam and computer facilities.

References

[1] R.D. Field and R.P. Feynman, Nucl. Phys. B136 (1978) 1.

[2] B. Andersson et al., Phys. Rep. 97 (1983) 31.

[3] B.R. Webber, Nucl. Phys. B238 (1983) 492;
R.D. Field, Phys. Lett. 135B (1984) 203.

[4] H.E. Montgomery, Proceedings of the 1981 International Symposium on Lepton and Photon Interactions at High Energies, Bonn (edited by W. Pfeil, Bonn, FRG 1981), p. 508.

[5] EMC, J.J. Aubert et al., Phys. Lett. 103B (1981) 388;
EMC, J.J. Aubert et al., Phys. Lett. 135B (1984) 225.

[6] JADE, W. Bartel et al., Phys. Lett. 104B (1981) 325;
TASSO, M. Althoff et al., Z. Phys. C17 (1983) 5;
TASSO, M. Althoff et al., Phys. Lett. 139B (1984) 126.

[7] H. Aihara et al., Phys. Rev. Lett. 52 (1984) 577;
H. Aihara et al., Phys. Rev. Lett. 53 (1984) 130;
H. Aihara et al., Phys. Rev. Lett. 54 (1985) 274;
H. Aihara et al., Phys. Rev. Lett. 55 (1985) 1047;
C. de la Vaissiere et al., Phys. Rev. Lett. 54 (1985) 2071;
M. Derrick et al., PU-85-537, submitted to Phys. Rev. D.

[8] B. Andersson et al., Z. Phys. C13 (1982) 361.

[9] B. Andersson, G. Gustafson, T. Sjöstrand,
Physica Scripta 32 (1985) 574.

[10] A. Casher et al., Phys. Rev. D20 (1979) 179.

[11] EMC, M. Arneodo et al., Phys. Lett. 145B (1984) 156;
EMC, M. Arneodo et al., CERN-EP/86-160, to be published in Z. Phys. C.

[12] EMC, M. Arneodo et al., Phys. Lett. 150B (1985) 458;
EMC, M. Arneodo et al., Nucl. Phys. B264 (1986) 739.

[13] T. Sjöstrand, Comput. Phys. Commun. 39 (1986) 347;
G. Ingelman, private communication.

[14] EMC, O.C. Allkhofer et al.,
Nucl. Instrum. Methods 179 (1981) 445;
EMC, J.P. Albanese et al.,
Nucl. Instrum. Methods 212 (1983) 111.

[15] S. Fredriksson, M. Jändel, T.I. Larsson,
Phys. Rev. Lett. 51 (1983) 2179.

[16] EMC, M. Arneodo et al., Nucl. Phys. B258 (1985) 249;
EMC, M. Arneodo et al., Z. Phys. C31 (1986) 1.

[17] EMC, J.J. Aubert et al., Phys. Lett. 123B (1983) 123.

[18] TPC/Two-Gamma Collaboration, H. Aihara et al.,
Phys. Rev. Lett. 57 (1986) 3140.

Table 1

Numbers of events, identified protons (p) and antiprotons ($\bar{p}$) from the H_2 and the D_2 target as found in the raw data. The numbers of misidentified protons (BG(p)) and antiprotons (BG($\bar{p}$)) are estimated from the Monte Carlo. For the background only the statistical errors caused by the limited statistics in the Monte Carlo simulation are quoted.

	Events	p	BG (p)	$\bar{p}$	BG ($\bar{p}$)
H_2	25047	3421	800 ± 14	981	260 ± 8
D_2	20788	2497	710 ± 15	829	239 ± 9

Table 2

Numbers of identified pp, $p\bar{p}$ and $\bar{p}\bar{p}$ pairs as found in the raw data and number of falsely identified combinations (background) estimated from Monte Carlo calculations.

		Identified Pairs	Background Pairs
pp	H_2	164	77 ± 4
	D_2	92	50 ± 3
$p\bar{p}$	H_2	227	73 ± 4
	D_2	147	56 ± 4
$\bar{p}\bar{p}$	H_2	20	6 ± 1
	D_2	16	7 ± 1

Table 3

Average multiplicities of pp, $p\bar{p}$ and $\bar{p}\bar{p}$ combinations and R (as defined in section 5) for the data and the Lund model prediction. Note that the experimental values are only corrected for acceptance in the limited momentum ranges where protons can be identified. The same momentum cuts have been applied to the model predictions. The statistical errors in the Lund model prediction for pp and $p\bar{p}$ pairs are negligible.

		$\langle n_{ij} \rangle \cdot 10^3$		R	
		Data	Lund	Data	Lund
pp	H_2	35 ± 5	42	0.232 ± 0.036	0.238
	D_2	22 ± 5	29	0.184 ± 0.044	0.260
	combined	29 ± 4		0.212 ± 0.028	
$p\bar{p}$	H_2	37 ± 4	69	1.14 ± 0.12	1.69
	D_2	40 ± 6	59	1.11 ± 0.17	1.81
	combined	38 ± 3		1.13 ± 0.10	
$\bar{p}\bar{p}$	H_2	2.0 ± 0.6	0.85 ± 0.09	1.16 ± 0.38	0.36 ± 0.04
	D_2	2.1 ± 1.0	0.80 ± 0.15	0.78 ± 0.36	0.35 ± 0.06
	combined	2.0 ± 0.5		0.96 ± 0.26	

Figure Captions

1) Acceptance of the detector for protons and antiprotons vs. laboratory momentum (a) and vs. x_F (b).

2) Background to signal ratio for protons (full line) and antiprotons (dashed line) vs. laboratory momentum (a) and vs. x_F (b). Only the full line is drawn in the regions where the ratios for protons and antiprotons are the same.

3) x_F distributions for protons (circles) and antiprotons (triangles) from the H_2 (full symbols) and the D_2 target (open symbols). The curves show the Lund model predictions (full line: p from H_2, dashed: p from D_2, dashed-dotted: $\bar{p}$ from H_2/D_2).

4) Rapidity distribution of the total proton number $N_p - N_{\bar{p}}$ for four x_{Bj} intervals: a) $x_{Bj} < 0.035$, b) $0.035 \leq x_{Bj} < 0.1$, c) $0.1 \leq x_{Bj} < 0.2$ and d) $0.2 \leq x_{Bj}$. The data from the H_2 and the D_2 targets are combined. The curves show the Lund model predictions (full line: H_2, dashed line: D_2 target).

5) Average multiplicities from the H_2 (full circles) and the D_2 target (open circles) vs. W for backward protons (a), backward antiprotons (b), forward protons (c) and forward antiprotons (d). The histograms show the Lund model predictions (full line: H_2 target, dashed line: D_2 target, full line only where both are the same).

6) Ratios of the average multiplicities of backward protons (a), forward protons (b) and antiprotons (c) from the H_2 to the D_2 target vs. x_{Bj}. The Lund model predictions are shown by the histograms.

7) Ratio of the normalised rapidity distributions of protons from events with an antiproton to all events. The data from the H_2 and the D_2 target are combined. The Lund model prediction for a hydrogen target is shown by the histogram. The data are corrected only for acceptance in the momentum range where proton identification is possible (see fig. 1). The same cuts are applied to the Lund model prediction.

8) Rapidity gap distributions for pp pairs (a), $p\bar{p}$ pairs with $y_p < -1$ (b) and $p\bar{p}$ pairs with $y_p > 0.5$ (c). The data from both targets are combined. The Lund model predictions, calculated for a hydrogen target, are shown by the histograms. The data and the model are treated as in fig. 7.

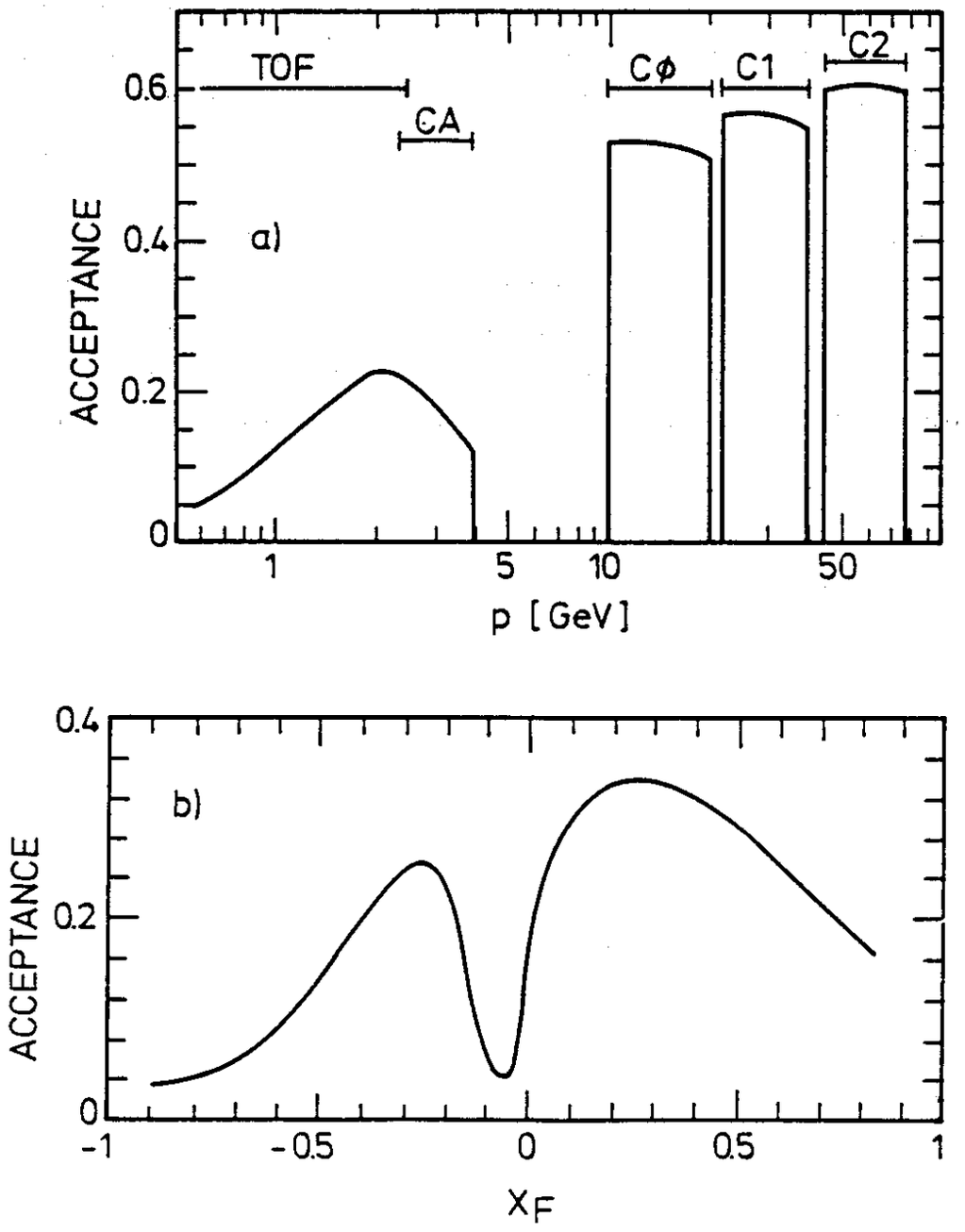
TOF
CA
Cφ
C1
C2
a)
ACCEPTANCE
0.6
0.4
0.2
0
1
5
10
50
p [GeV]
b)
ACCEPTANCE
0.4
0.2
0
-1
-0.5
0
0.5
1
X_F

Fig. 1

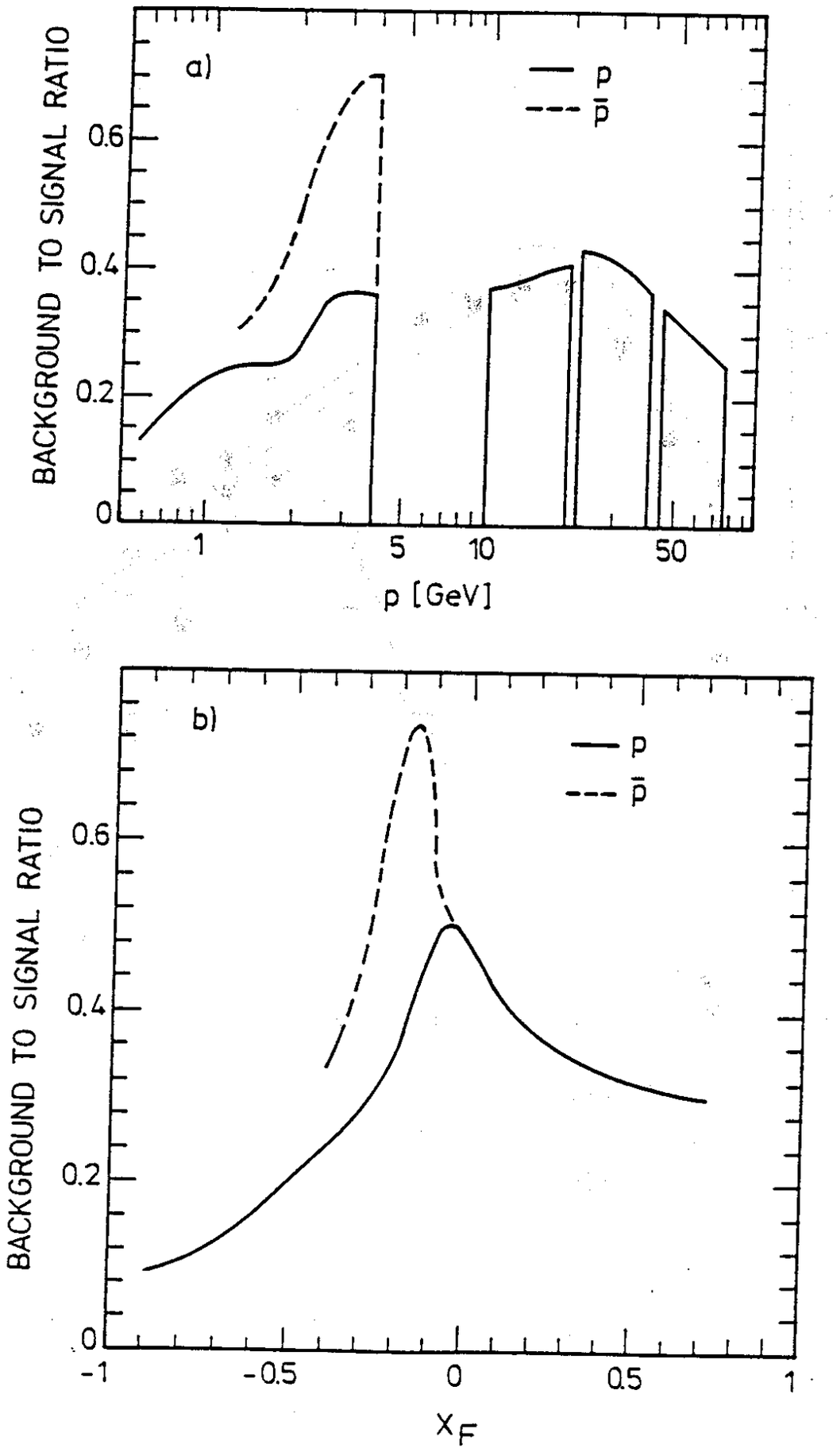
a)
p
p̄
BACKGROUND TO SIGNAL RATIO
0
0.2
0.4
0.6
1
5
10
50
p [GeV]
b)
p
p̄
BACKGROUND TO SIGNAL RATIO
0
0.2
0.4
0.6
-1
-0.5
0
0.5
1
x_F

Fig. 2

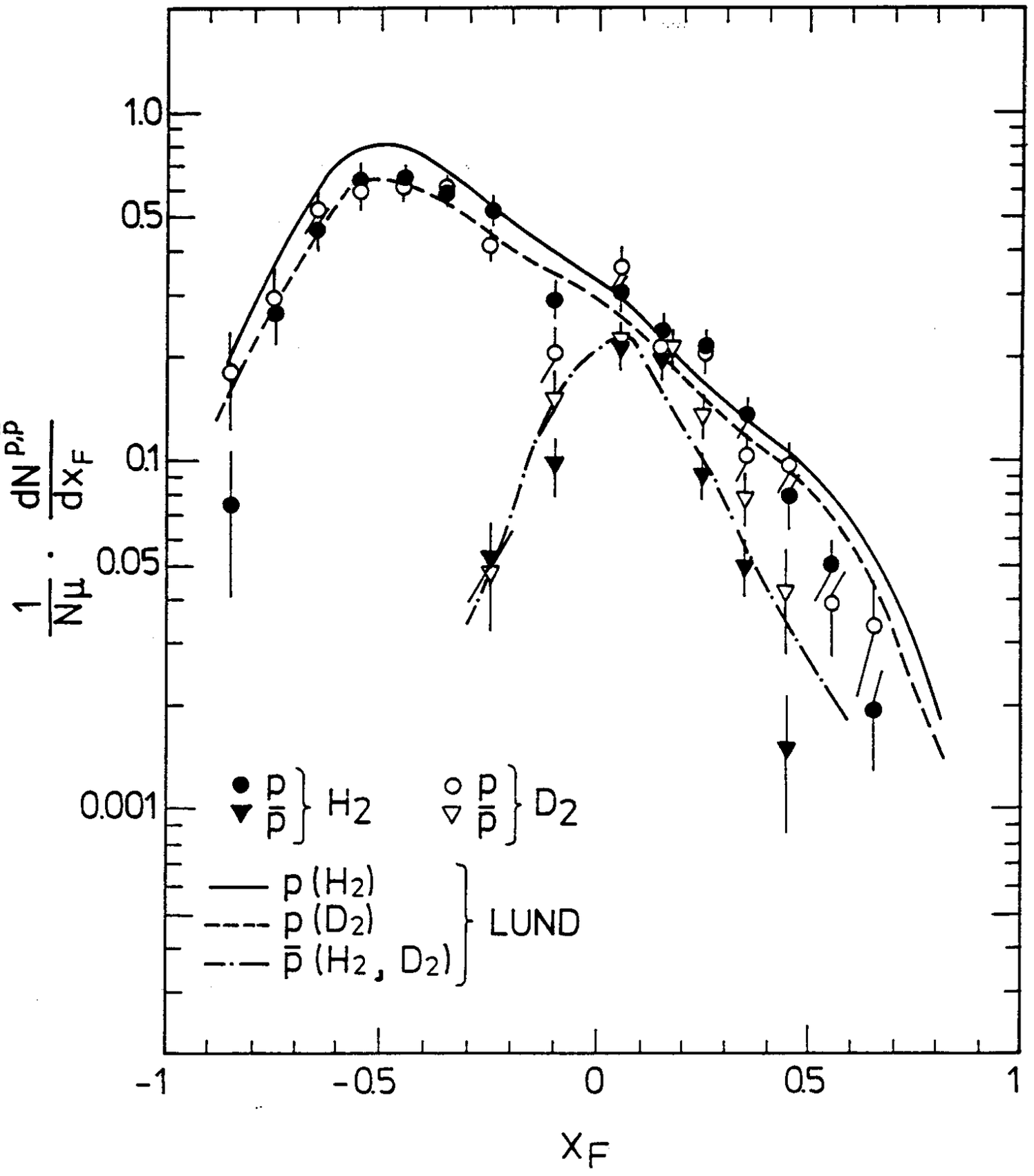
1.0
0.5
0.1
0.05
0.001
$\frac{1}{N\mu} \cdot \frac{dN^{p,\bar{p}}}{dx_F}$
p
$\bar{p}$
H_2
p
$\bar{p}$
D_2
p (H_2)
p (D_2)
$\bar{p}$ (H_2, D_2)
LUND
-1
-0.5
0
0.5
1
x_F

Fig. 3

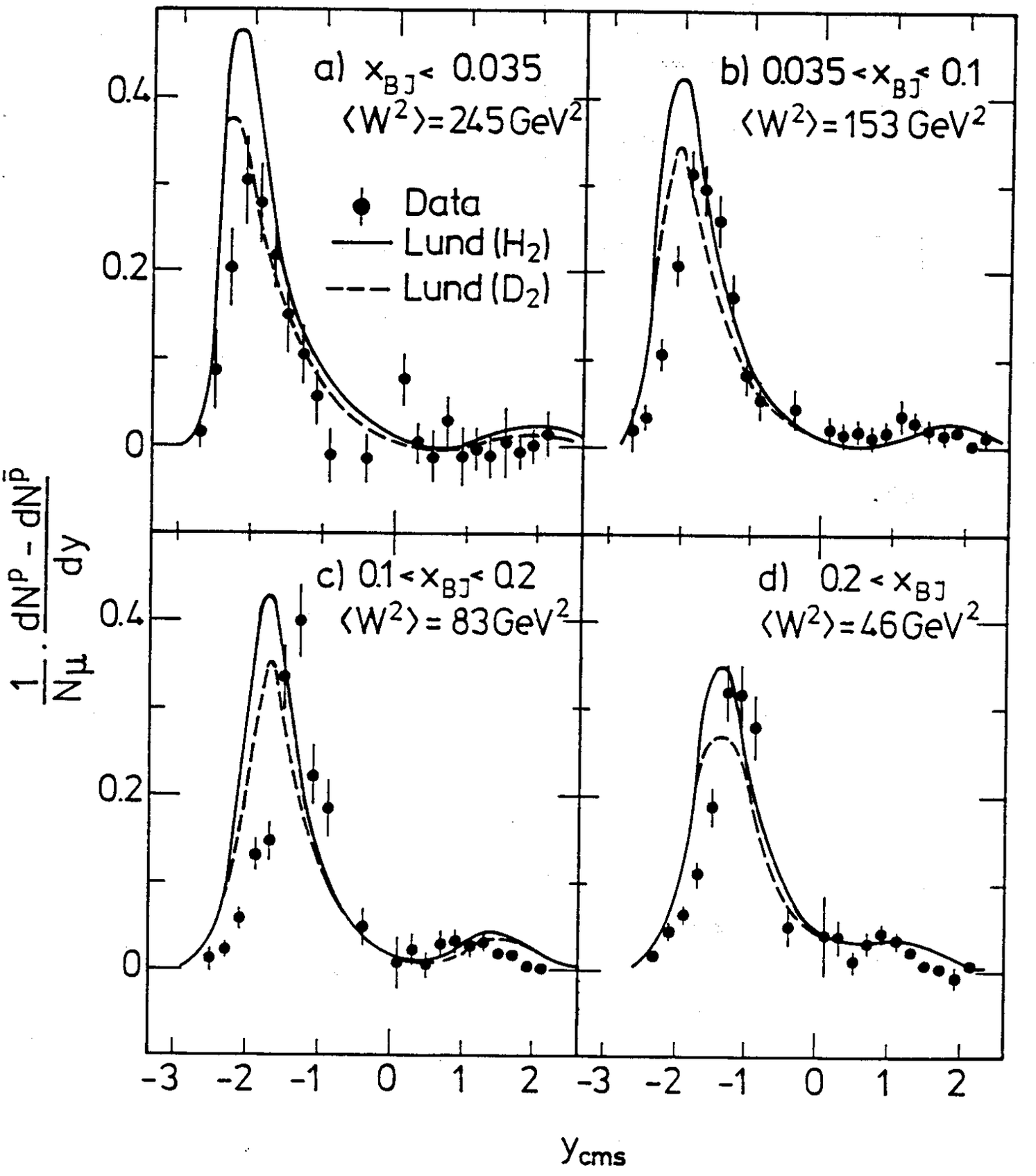
a) $x_{BJ} < 0.035$
$\langle W^2 \rangle = 245\,GeV^2$
b) $0.035 < x_{BJ} < 0.1$
$\langle W^2 \rangle = 153\,GeV^2$
c) $0.1 < x_{BJ} < 0.2$
$\langle W^2 \rangle = 83\,GeV^2$
d) $0.2 < x_{BJ}$
$\langle W^2 \rangle = 46\,GeV^2$
Data
Lund (H_2)
Lund (D_2)
$\frac{1}{N\mu} \cdot \frac{dN^p - dN^{\bar{p}}}{dy}$
y_{cms}

Fig. 4

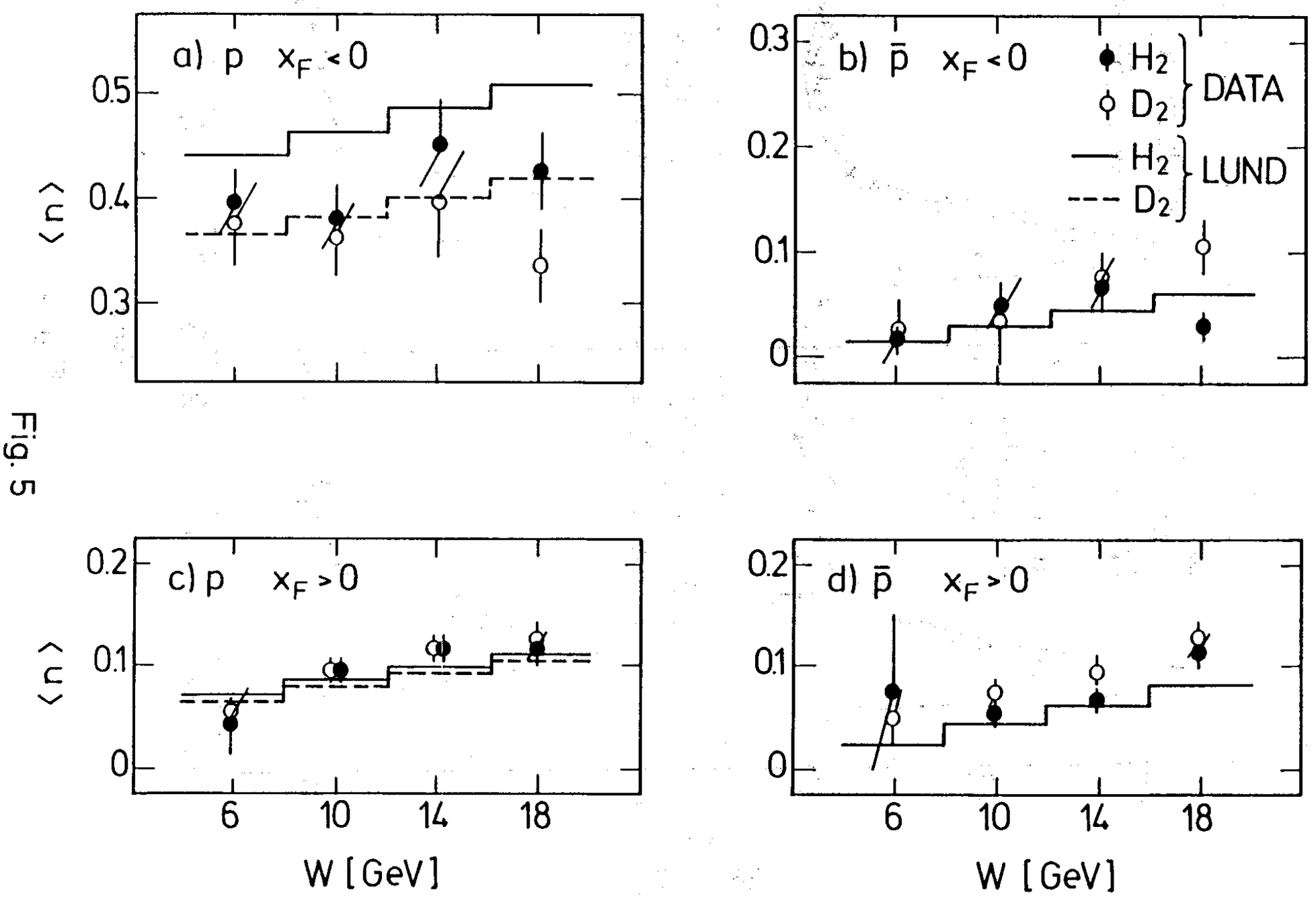
a) p $x_F < 0$
b) $\bar{p}$ $x_F < 0$
H_2
D_2
DATA
LUND
c) p $x_F > 0$
d) $\bar{p}$ $x_F > 0$
$\langle n \rangle$
W [GeV]

Fig. 5

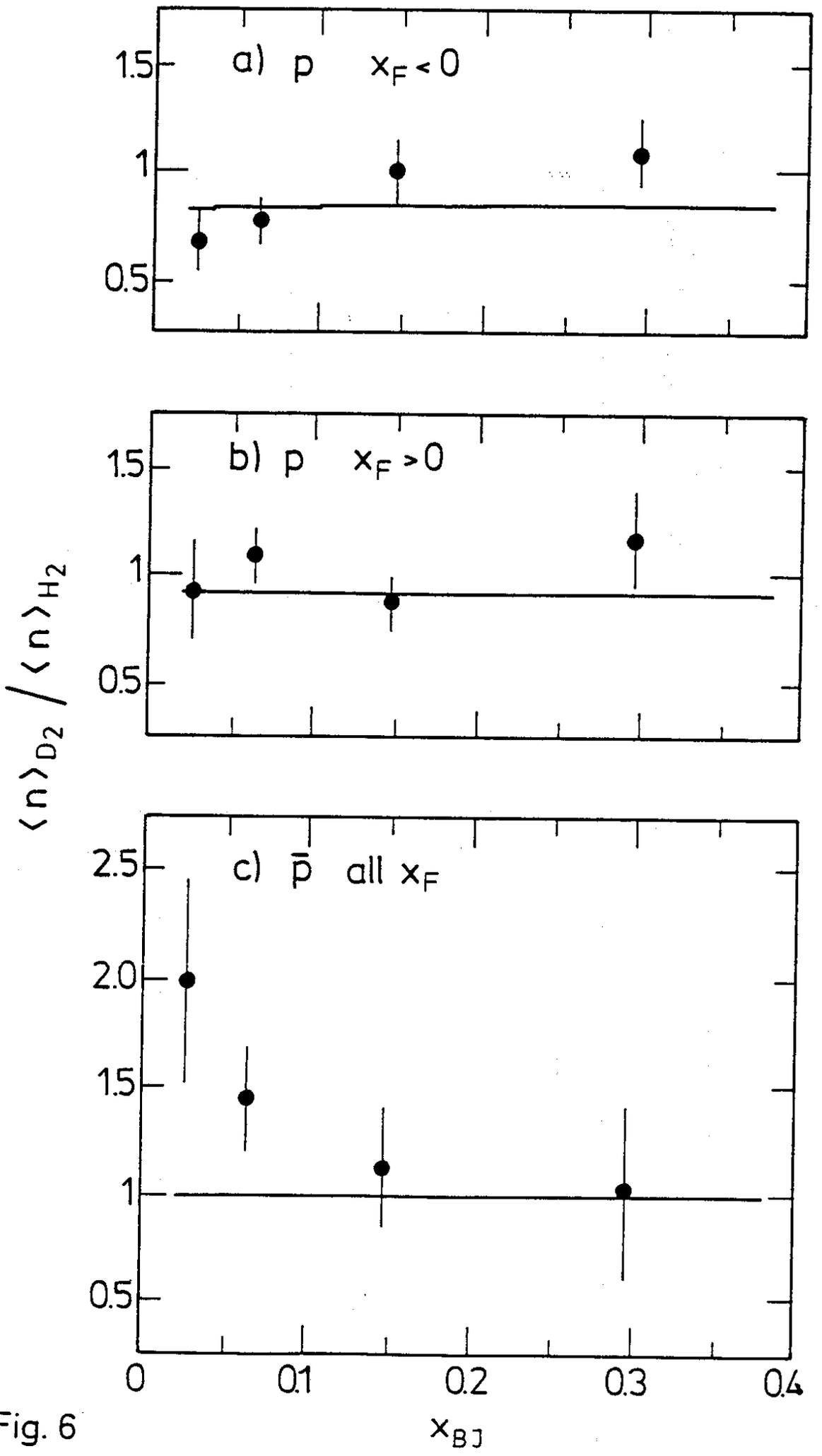
a) p $x_F < 0$
b) p $x_F > 0$
c) $\bar{p}$ all x_F
1.5
1
0.5
2.5
2.0
0
0.1
0.2
0.3
0.4
$\langle n \rangle_{D_2} / \langle n \rangle_{H_2}$
x_{BJ}

Fig. 6

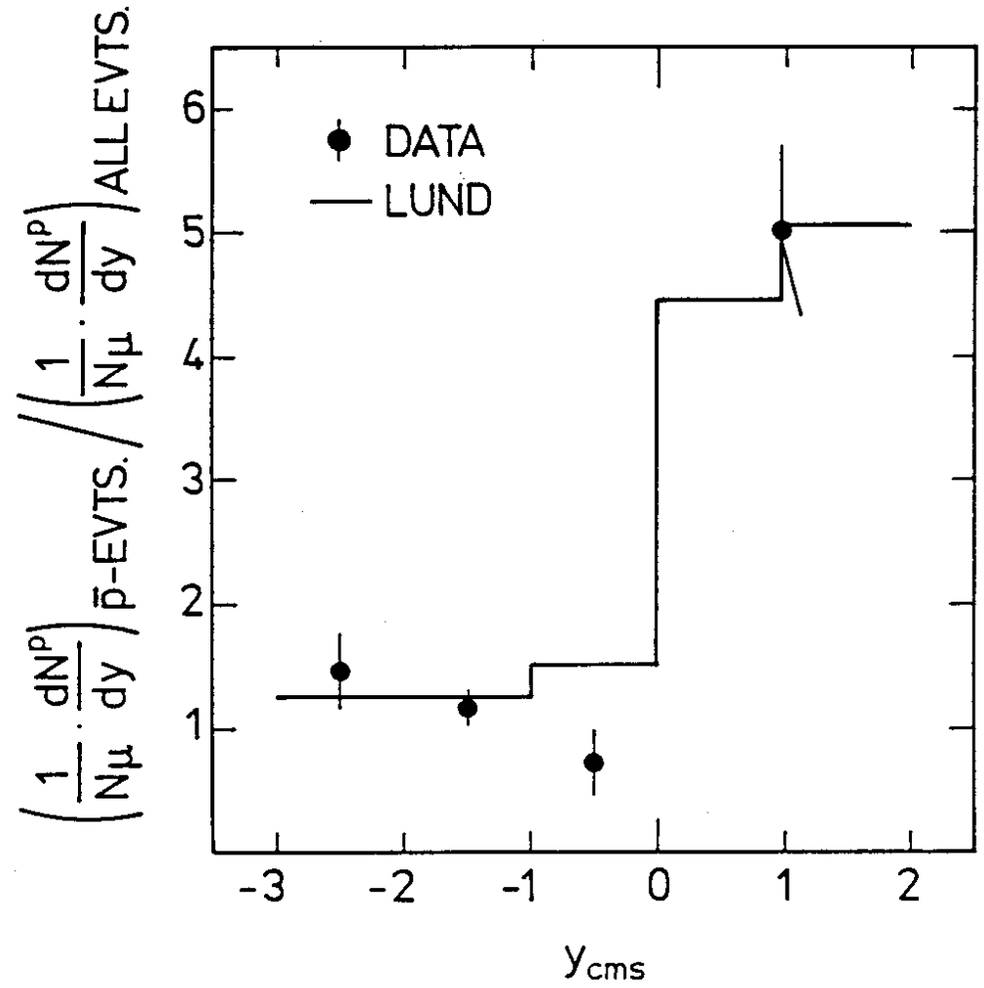
DATA
LUND
$\left(\frac{1}{N\mu}\cdot\frac{dN^p}{dy}\right)_{\bar{p}\text{-EVTS.}} \Big/ \left(\frac{1}{N\mu}\cdot\frac{dN^p}{dy}\right)_{\text{ALL EVTS.}}$
y_{cms}

Fig. 7

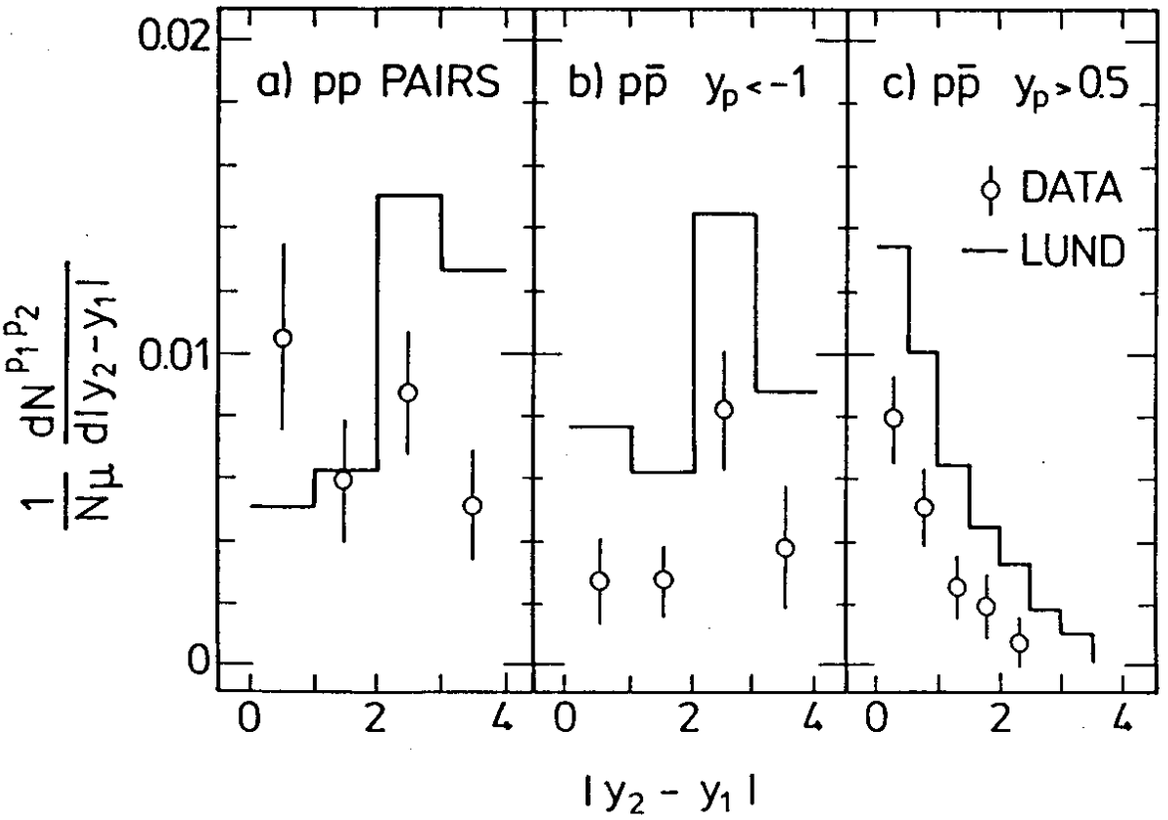
a) pp PAIRS
b) $p\bar{p}$ $y_p < -1$
c) $p\bar{p}$ $y_p > 0.5$
DATA
LUND
$\frac{1}{N\mu}\frac{dN^{p_1p_2}}{d|y_2-y_1|}$
$|y_2 - y_1|$

Fig. 8